ACS APPLIED MATERIALS & INTERFACES

Research Article

www.acsami.org

Naphthodithiophene-Based Conjugated Polymer with Linear, Planar Backbone Conformation and Strong Intermolecular Packing for Efficient Organic Solar Cells

Jaewon Lee, Hyomin Ko, Eunjoo Song, Heung Gyu Kim, and Kilwon Cho*

Department of Chemical Engineering, Pohang University of Science and Technology, Pohang, 790-784, Korea

Supporting Information

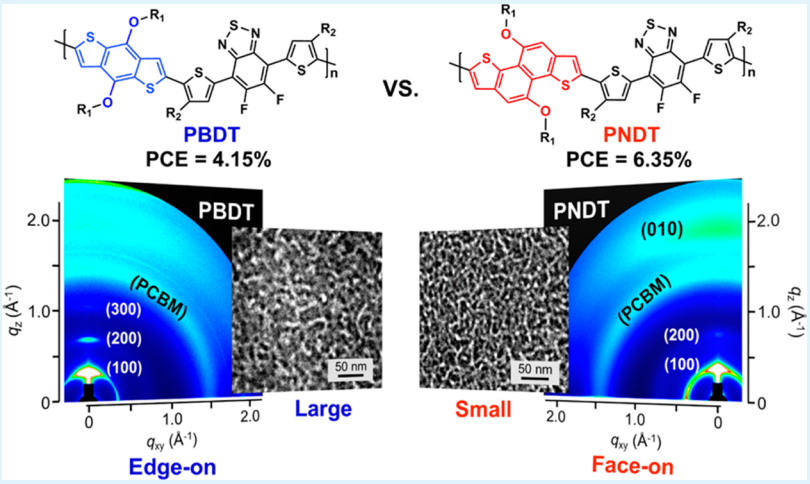

ABSTRACT: Two donor−acceptor copolymers, PBDT and PNDT, containing 4,8-bis(2-ethylhexyloxy)benzo[1,2-b:3,4-b′]dithiophene (BDT) and 4,9-bis(2-ethylhexyloxy)naphtho[1,2-b:5,6-b′]dithiophene (NDT), respectively, as an electron-rich unit and 5,6-difluoro-2,1,3-benzothiadiazole (2FBT) as an electron-deficient unit, were synthesized and compared. The introduction of the NDT core into the conjugated backbone was found to effectively improve both light harvesting and the charge carrier mobility by enhancing chain planarity and backbone linearity; the NDT copolymer has stronger noncovalent interactions and smaller bond angles than those of the BDT-based polymer. Moreover, the introduction of the NDT core brings about a drastic change in the molecular orientation into the face-on motif and results in polymer:PCBM blend films with well-mixed interpenetrating nanofibrillar bulk−heterojunction networks with small-scale phase separation, which produce solar cells with higher short-circuit current density and fill factor values. A conventional optimized device structure containing PNDT:$PC_{71}BM$ was found to exhibit a maximum solar efficiency of 6.35%, an open-circuit voltage of 0.84 V, a short-circuit current density of 11.92 mA cm^{-2}, and a fill factor of 63.5% with thermal annealing, which demonstrates that the NDT and DT2FBT moieties are a promising electron-donor/acceptor combination for high-performance photovoltaics.

KEYWORDS: *polymer solar cells, naphtho[1,2-b:5,6-b′]dithiophene, benzo[1,2-b:3,4-b′]dithiophene, backbone planarity, bulk−heterojunction networks*

1. INTRODUCTION

Over the past few years, there has been remarkable progress in the technology of polymer solar cells (PSCs), such as in the development of new organic semiconductors,[1−3] improvements in an understanding of device operation mechanisms,[4] the engineering of new device architectures,[5−7] and the optimization of processing techniques.[8,9] The most promising device performances have been achieved with active layers in bulk−heterojunction (BHJ) networks[10,11] of interpenetrated π-conjugated polymer electron donors and fullerene electron acceptors; their power conversion efficiencies (PCEs) exceed 10% in single-junction devices.[12−14]

To further improve PCEs, the design of the molecular structure of the low band gap (LBG) polymer is crucial, and particular consideration of its close relationship with photovoltaic parameters, including the short-circuit current density (J_{SC}), the open-circuit voltage (V_{OC}), and the fill factor (FF), is required. Recently, the acenedithiophene family (AcDT), such as benzodithiophenes (BDTs),[15] naphthodithiophenes (NDTs),[16] and anthradithiophenes (ADTs),[17] have been extensively incorporated into a variety of conjugated polymers

Received: June 5, 2015
Accepted: September 11, 2015
Published: September 11, 2015

DOI: 10.1021/acsami.5b04884
ACS Appl. Mater. Interfaces 2015, 7, 21159−21169

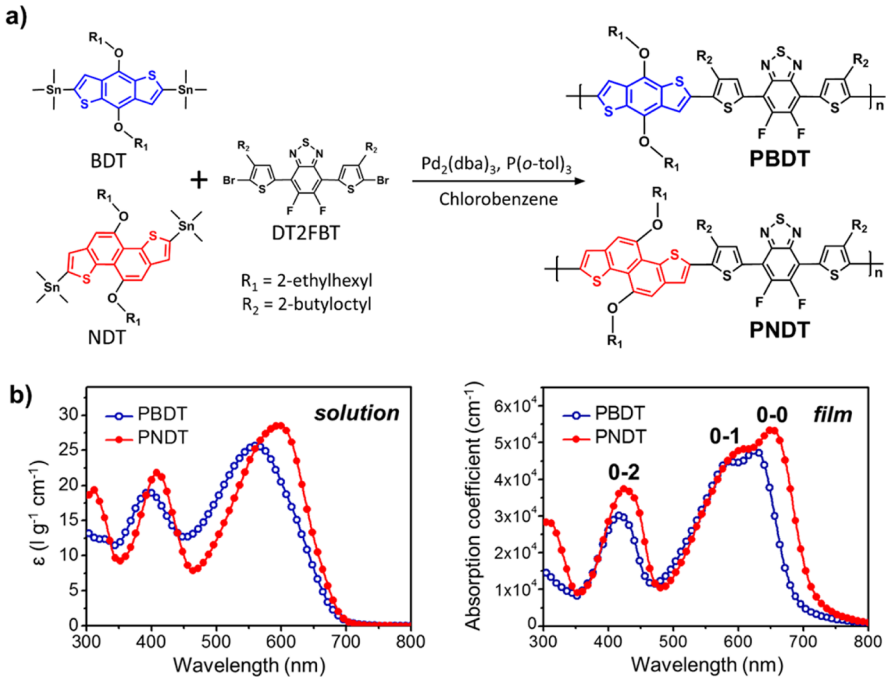

Figure 1. (a) Synthesis and chemical structure of PBDT and PNDT copolymers. Conditions: $Pd_2(dba)_3$, P(*o*-tol)$_3$, chlorobenzene, 110 °C for 48 h. (b) UV−vis absorption spectra of polymers in DCB at a concentration of 0.025 g L^{-1} for 25 °C and spin-coated thin films prepared by DCB.

to produce high-performance organic field-effect transistors (OFETs) and PSCs.[18−22] The fused and symmetric structure of AcDT produces a high degree of backbone coplanarity and the regular packing of the intermolecular polymer chain, which facilitates π-electron delocalization and induces strong $\pi-\pi$ stacking for efficient charge transport. The ease of regioselective functionalization at the α-positions of the two outer thiophenes of AcDTs imparts structural versatility and enables precise cross-coupling polymerization.[16] Furthermore, the alkylation of the AcDT units is facile, which provides ease of control over the solubility and molecular orientation of the resultant semiconducting polymers and thus over the BHJ morphologies of photoactive layers.[15]

NDT has recently attracted great interest as a donor core for organic semiconductors. In comparison to BDT, NDT has a more extended π-conjugated system and a larger planar heteroarene structure, which leads to enhanced π-orbital overlapping, strong intermolecular interactions, and efficient charge transport.[16] Furthermore, NDT has greater structural modification versatility than BDT because there are more open sites on the central naphthalene unit in NDT. On the basis of the diversity of practical synthetic routes for NDT units, various classes of NDT-based organic semiconductors have been developed.[23] NDT units have been extensively used as building blocks for OFETs, both small molecules and polymers.[24] NDT-based semiconductors exhibit higher charge carrier mobilities than their BDT-based counterparts in OFETs. In spite of these promising characteristics, the use in polymer solar cells of NDT-based organic semiconductors has received much less attention than that of BDT-based semiconductors. Recently, a novel class of NDT-based photovoltaic copolymers with promising device performances, such as power conversion efficiencies greater than 8%, has been developed.[25−27] These results demonstrate the significant potential of the NDT core for high-performance photovoltaic materials.

In this study, we report a new NDT-based donor−acceptor (D−A) copolymer for use in solution-processable PSCs. We designed two D−A copolymers with different donor units, BDT and NDT, in order to investigate the effects of introducing AcDT units on the photophysical properties of polymers and PSC performance (Figure 1). PNDT consists of an angular NDT group flanked by two thiophene groups as a donor unit and difluorobenzothiadiazole (2FBT) as an acceptor unit. 2FBT was chosen as the acceptor unit because it has strong electron-withdrawing properties and allows backbone planarization because of the small size of the fluorine atoms.[27−29] The thermal, electrochemical, photophysical, and optoelectronic properties of the two D−A copolymers were systematically investigated by conducting experimental and theoretical measurements. PNDT was found to exhibit a PCE of 6.35% with strong light absorption and charge transport properties, whereas PBDT exhibits a PCE of 4.12%. Thus, the NDT building block in the D−A copolymer is very promising and comparable to or even more effective than the BDT building block for high-performance solar cells.

2. RESULTS AND DISCUSSION

2.1. Molecular Design, Synthesis, and Characterization. The monomers based on dialkoxynaphthodithiophene (NDT), dialkoxybenzodithiophene (BDT) and difluorobenzothiadiazole (2FBT), were prepared according to previously reported procedures.[18,21,29] The detailed synthetic procedures and characterization results for the monomers are presented in the Supporting Information (SI). Branched alkyl chains, 2-ethylhexyl and 2-butyloctyl, were employed to ensure the solubility of the target polymers. The target copolymers shown in Figure 1a were prepared through Stille cross-coupling reactions between bis(trimethyltin) (BDT) (or NDT) and the dibrominated DT2FBT under nearly the same conditions. The crude products were isolated in chloroform after Soxhlet extraction with methanol, acetone, or hexanes. After Soxhlet

DOI: 10.1021/acsami.5b04884
ACS Appl. Mater. Interfaces 2015, 7, 21159−21169

Table 1. Characteristics of PBDT and PNDT

				HOMO/LUMO (eV)				
polymer	$\overline{M_n}/\overline{M_w}$ (kDa)[a]	PDI (M_w/M_n)[a]	T_d (°C)[b]	DFT	cyclic voltammetry	$\lambda_{max}^{sol.}$ (nm)[c]	λ_{max}^{film} (nm)[d]	E_g^{opt} (eV)[e]
PBDT	27.4/64.6	2.36	338	−4.84/−2.94	−5.46/−3.66	561	578, 627	1.76
PNDT	33.8/114.9	3.40	347	−4.77/−3.25	−5.32/−3.60	597	602, 654	1.66

[a]Determined by GPC using polystyrene standards and CB as eluent. [b]5% weight loss temperatures measured by TGA under nitrogen atmosphere. [c]Measured in dilute DCB solution at a concentration of 0.05 g L^{-1}. [d]Spin-cast from 10 mg mL^{-1} DCB solution. [e]Estimated from the onset of the UV−vis spectra measured from thin films.

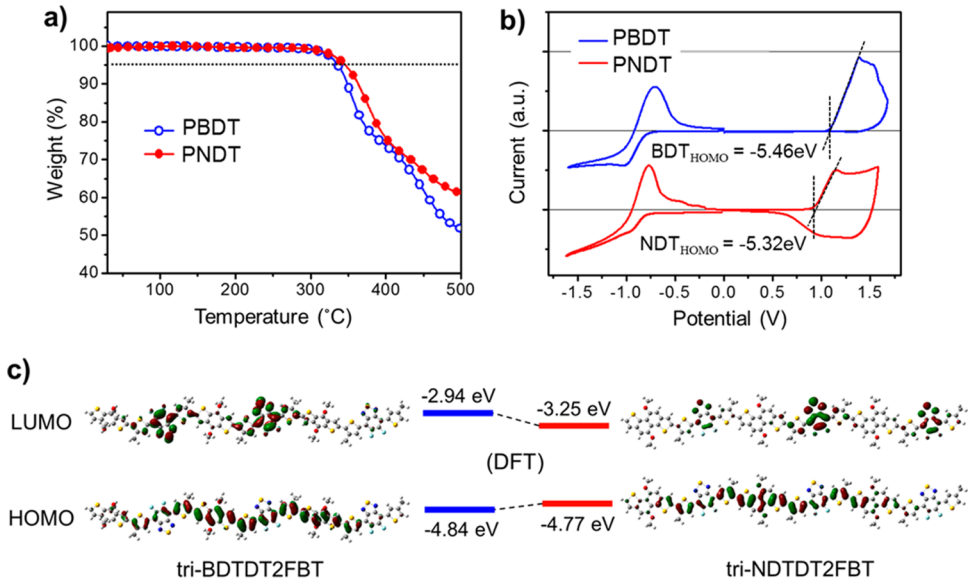

Figure 2. (a) TGA plots of polymers with a heating rate of 10 °C min^{-1} under an inert atmosphere. (b) Cyclic voltammograms of polymers in CH_3CN solution at a scan rate of 50 mV s^{-1}. (c) Frontier molecular orbital and energy level diagrams dererminded by DFT calculation (B3LYP functional/6-21G* basis set).

extraction, the copolymers were washed in sodium diethyldithiocarbamate trihydrate to extract as much residual palladium as possible before being precipitated into methanol.[30] Finally, the copolymers were precipitated into methanol and dried. Both polymers were found to exhibit reasonable solubility in common organic solvents, such as chloroform (CF), chlorobenzene (CB), and 1,2-dichlorobenzene (DCB), upon warming. The number-average molecular weights ($\overline{M_n}$) of the resulting polymers were 27.4 and 33.8 kDa, respectively, with polydispersity indexes (PDIs) of 2.36 and 3.40 (Table 1).

2.2. Optical Properties. The UV−vis absorption spectra of the BDT- and NDT-based copolymers were measured in dilute DCB solutions at room temperature and as thin films spin-coated from a solution of DCB (10 mg mL^{-1}) (Figure 1b). The detailed absorption data, including the absorption maxima and band edges, are summarized in Table 1. The absorption spectra of the two copolymers contain two spectral features, a high-energy band attributed to the localized $\pi-\pi^*$ transition and a lower-energy band ascribed to the intracharge transfer (ICT) transition, which are similar to those of other copolymers comprising D−A units.[31]

Broad, featureless absorption spectra were recorded for the two polymers in DCB solution, which suggests that the polymer chains are isolated by the solvent molecules without polymer aggregation at a concentration of 0.05 mg mL^{-1}. There is a bathochromic absorption peak at 597 nm in the spectrum of PNDT (the peak is at 561 nm for PBDT) and the maximal absorption coefficient is 28.1 g^{-1} cm^{-1}. Although there is a significant red-shift for both polymers in the solid state, PNDT exhibits a wider and overall stronger absorption. The long wavelength onsets for the polymers are 706 and 748 nm, respectively, which correspond to optical band gaps (E_g) of 1.76 and 1.66 eV. Since the low-energy absorption band of a conjugated polymer in the visible region is assigned mainly to the ICT transition characteristic of the conjugated main chain,[18] this expanded absorption of PNDT is probably due to the extended π-conjugation length of the NDT building block.[32] The vibronic shoulder peaks of the two copolymers at 627 and 654 nm imply that their interchain $\pi-\pi^*$ transitions (A_{0-0}) are strong, which indicates that these polymers have structurally organized and orderly packed structures in the thin film state.[33] The vibronic absorption peak (the evolution of the A_{0-0}/A_{0-1} ratio) of PNDT has a higher intensity, probably because of more effective $\pi-\pi$ stacking between the polymer backbones.

2.3. Thermal and Electrochemical Properties. Differential scanning calorimetry (DSC) and thermogravimetric analysis (TGA) were performed for the two copolymers under an inert nitrogen atmosphere. The DSC results for the two copolymers contain no obvious transitions between 20 and 400 °C. The 5% mass loss of PBDT arises at 338 °C, whereas that of PNDT is at 347 °C (Figure 2a). In any case, the temperatures at which the decompositions occur are much higher than any annealing temperatures used in BHJ fabrication processes.

The electrochemical properties of both polymers were investigated by performing cyclic voltammetry (CV) measure-

DOI: 10.1021/acsami.5b04884
ACS Appl. Mater. Interfaces 2015, 7, 21159−21169

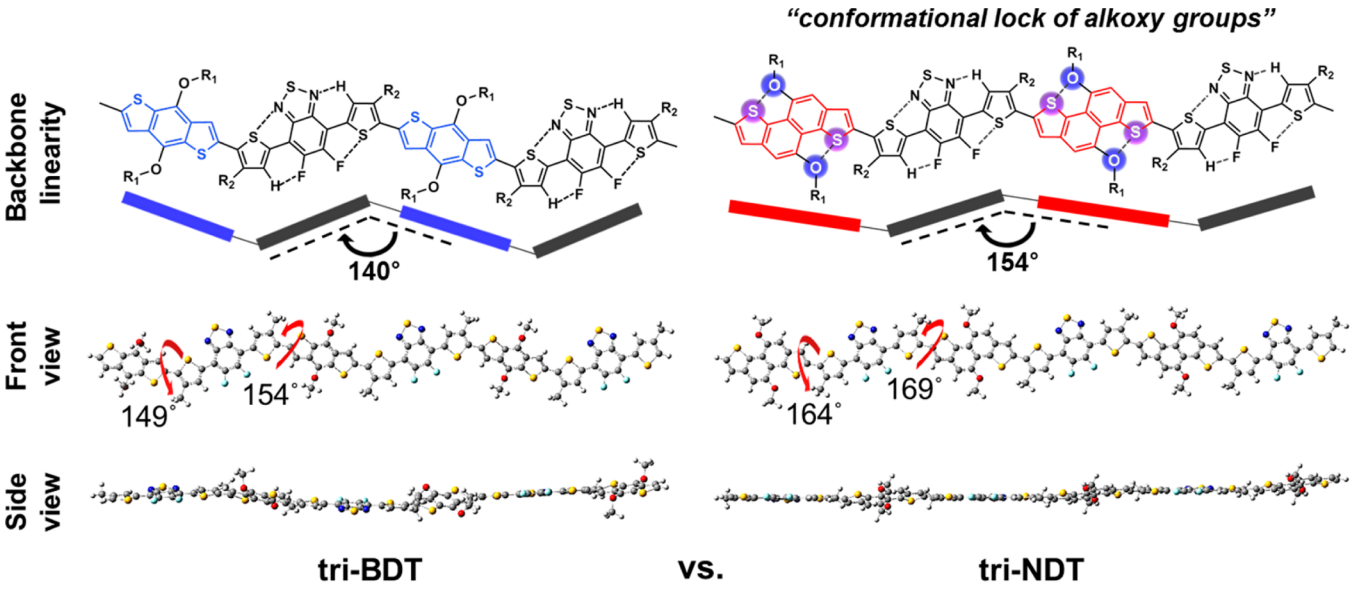

Figure 3. Illustration of the structural conformation of tri-BDT and tri-NDT. Dihedral angle and backbone planarity of trimers for PBDT and PNDT were measured by DFT calculation (B3LYP functional/6-21G* basis set). θ* is a key dihedral angle determining the backbone planarity.

Table 2. OFET Performance and Crystallographic Information of Pristine Polymer Films

polymer	$\mu_{h/av}$ ($cm^2\ V^{-1}\ s^{-1}$)[a]	I_{on}/I_{off}	d^{100} (Å)[b]	fwhm^{100} ($Å^{-1}$)[c]	$L_C{}^{100}$ (nm)[d]	d^{010} (Å)[b]	fwhm^{010} ($Å^{-1}$)[c]	$L_C{}^{010}$ (nm)[d]
PBDT	4.0×10^{-4}	2.0×10^{4}	18.5	0.115	4.90	4.1	0.341	1.65
PNDT	1.9×10^{-3}	4.8×10^{5}	17.4	0.081	6.95	3.8	0.240	2.35

[a]The p-channel characteristics of OFETs were measured with $V_{DS} = -60$ V ($L = 150$ μm and $W = 1500$ μm). [b]Domain spacings of lamellar (d^{100}) and $\pi-\pi$* (d^{010}) stacking in neat polymer films in the out-of-plane (q_z) direction. [c]Full width at half-maximum (fwhm) values. [d]Correlation lengths (L_C) of lamellar and $\pi-\pi$* stacked crystals using the Scherrer equation.

ments (Figure 2b). The highest occupied molecular orbital/lowest unoccupied molecular orbital (HOMO/LUMO) values of PBDT and PNDT were calculated on the basis of the onsets of the redox potentials by using the known energy level of ferrocene, which is 4.8 eV below the vacuum level (Table 1). PBDT and PNDT have deep-lying HOMO levels of −5.46 and −5.32 eV, respectively, which suggest high oxidization and device stabilities. The HOMO level of PNDT is higher than that of PBDT because of its lower band gap, as confirmed by the UV−vis absorption results.

2.4. Theoretical Calculations. Quantum mechanical calculations were performed to further investigate the geometric and electronic properties of these polymers. Density functional theory (DFT) calculations with the B3LYP/6-31G* model[34−36] were performed on trimers (tri-BDTDT2FBT and tri-NDTDT2FBT) based on the parent polymers by using same methyl-trimmed alkyl chains for simplicity of computation. The theoretical energy levels and energy gaps of the model structures are summarized in Table 1. Note that the trends of the theoretical results for the model compounds are in accordance with the relevant experimental results, even though the results differ with respect to actual values in the conjugated polymer systems, which is attributed to the limitations of the DFT models with trimmed alkyl side chains and a limited backbone length.[36]

For both trimers, the HOMO wave functions are well-delocalized along the conjugated backbone, whereas their LUMO wave functions are more localized on the acceptor unit (Figure 2c). A longer delocalization of the HOMO wave function was observed for tri-NDT than for tri-BDT. This increased orbital overlap of the NDT conjugated system can contribute to enhanced light absorption and charge transportation.[18] The computed values clearly indicate that the NDT-based trimer has a lower E_g than the BDT-based molecule. The theoretical HOMO/LUMO level results for the two trimers are in accordance with the relevant experimental results calculated from the CV data (Figure 2b). The optimized geometries of both trimers were investigated. Figure 3 shows that the backbone curvature of tri-NDT is more linear (≈154°) than that of tri-BDT (≈140°), which indicates that the NDT-based polymer has a high probability of a rigid backbone conformation in the solid state. Furthermore, tri-NDT has a more planar backbone conformation with smaller torsion angles (>11°) compared to tri-BDT (>26°), which is expected to facilitate π-electron delocalization and enhance charge mobility (Figure 3 and Figure S5, SI). The incorporation of the 2FBT unit produces noncovalent attractive interactions, such as C−H···N, C−H···F, N···S, O···S, and F···S,[37] and thus promotes excellent planarity with respect to the neighboring thienyl groups in both conjugated backbones.

However, noncovalent S−O attractive interactions are more likely to arise in the NDT building blocks, in contrast to the BDT building blocks, because the sulfur and oxygen atoms in the NDT building blocks can get closer to each other in terms of atomic distance, compared to those in the BDT building blocks, owing to the zigzag conformation[21] and alkoxy-substituent position[15] of the alkoxy-NDT building blocks. These noncovalent attractive interactions between S (in the NDT building blocks) and O (in the alkoxy groups) can suppress excessive molecular steric hindrances of the alkoxy side chains, which can enhance an intermolecular chain packing

DOI: 10.1021/acsami.5b04884
ACS Appl. Mater. Interfaces 2015, 7, 21159−21169

and facilitate an interchain charge transportation of NDT-based polymer in the bulk thin films.

2.5. Hole Mobility and Crystalline Structures. Carrier mobility plays an important role in the performance of a polymer solar cell because it is directly related to charge transport and recombination.[38] To explore the correlations between rotational disorder, backbone linearity, and charge carrier mobility, PBDT- and PNDT-based OFETs were fabricated with a bottom-gate, top-contact device configuration by using evaporated gold as the source and drain electrodes.[39] The electrical performances of the OFETs are summarized in Table 2, and their transfer and output characteristics are shown in Figure S6 (SI). The calculated mobilities of PBDT and PNDT are 4.0×10^{-4} and 1.9×10^{-3} cm^2 V^{-1} s^{-1} with on/off ratios of 2.0×10^4 and 4.8×10^5, respectively. The higher hole mobility of PNDT clearly indicates the effectiveness of the covalently extended conjugation length of the NDT unit, which improves the backbone planarity and interchain packing of the copolymer.[40]

A high degree of crystallinity in a conjugated polymer in the film state correlates with a high hole mobility, which is an important requirement for an effective photovoltaic polymer. Grazing-incidence wide-angle X-ray scattering (GIWAXS) measurements were carried out to characterize the crystalline structures and molecular orientations of the polymers in the neat films. The two-dimensional scattering profiles and the out-of-plane and the in-plane profiles of these two polymer films using the GIWAXS measurement are shown in Figure 4. The

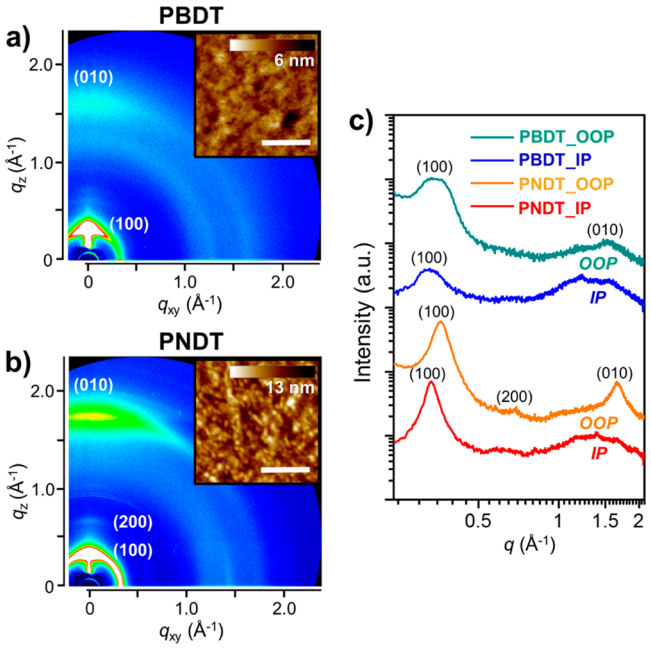

Figure 4. 2D GIWAXS pattern and AFM images of (a) PBDT and (b) PNDT neat films. The scale bar in the AFM images is 200 nm. (c) 1D GIWAXS plots of PBDT and PNDT neat films. OOP and IP indicate the out-of-plane and in-plane directions, respectively.

GIWAXS patterns of PBDT and PNDT indicate that the molecules in both neat polymer films are dominantly arranged with edge-on structures, but some face-on crystallites coexist. However, both the lamellar (q_z and q_{xy}, $h00$) and $\pi-\pi$ stacking (q_z, 010) diffractions of the PNDT film are much stronger than those of the PBDT film. It is worth mentioning that the d^{100} and d^{010} spacings of PNDT on the q_z axis are smaller than those of PBDT, which indicates that the crystallites of the PNDT polymer chains are more closely packed due to a more linear/coplanar structural conformation of PNDT (Table 2 and Figure 3). PNDT has the larger frame of the covalently π-extended building block, which provides more space per repeat unit and thus reduces the steric hindrance of the alkyl side chains. Further, the S−O attractive interactions of the NDT unit can suppress the steric hindrance of the alkoxy side chains. It can be concluded that the molecule has a more linear and planar conformation of the backbone by replacement of BDT with NDT, which is more favorable to form ordered interchain packing.[41]

Long-range packing order can be quantitatively measured by determining the correlation length (L_C) values of the crystals in the neat polymer films with the Scherrer equation; L_C is defined as the length over which a crystalline structure is preserved.[42] The PNDT film has larger L_C values (lamellar L_C^{100} and $\pi-\pi$ L_C^{010}) than PBDT film (Table 2); the larger L_C values of PNDT correspond to a narrower diffraction peak breadth.[43] This higher crystalline property of the PNDT film would facilitates intra- and interchain charge transport.

2.6. Photovoltaic Performance. We investigated the photovoltaic properties of both polymers in BHJ devices with a device configuration of ITO/PEDOT:PSS/polymer:$PC_{71}BM$/LiF/Al under an illumination intensity of AM 1.5G at 100 mW cm^{-2}. The D/A ratios (w/w), additive ratios (v/v), thermal annealing (TA) treatment, and active layer thicknesses of the two polymers were systematically varied to optimize device performance (see Tables S1 and S2, SI). DCB was chosen as the processing solvent for the deposition of the blend films since both polymers are readily soluble in DCB at low temperatures. The current−voltage ($J-V$) characteristics of the polymer solar cells are shown in Figure 5 and the relevant photovoltaic performance parameters are summarized in Table 3.

The devices with a conventional PSC architecture prepared without any posttreatments were found to exhibit PCEs of 1.35% and 4.12% for PBDT and PNDT, respectively. The optimal ratio of polymer:$PC_{71}BM$ for both polymer-based devices was 1:1 (Table 3). To further optimize the device performances of both polymers, we introduced a processing additive or performed thermal annealing treatment. For PBDT, the addition of 1,8-diiodooctane (DIO) to DCB (DCB:DIO = 98:2 by volume) was found to enhance the PCE remarkably from 1.35% to 4.15%. For PNDT, J_{sc} and FF were substantially improved by thermal annealing (150 °C for 10 min). The PSCs of PNDT prepared with thermal annealing were found to exhibit a J_{sc} of 11.9 mA cm^{-2}, a FF of 63.5%, and a PCE of 6.35%. The increases in the PCEs of both polymers after the DIO and TA treatments are closely related to morphological changes in their photoactive layers and improved contact between their active layers and electrodes,[14,44,45] which were confirmed with atomic force microscopy (AFM) and transmission electron microscopy (TEM) (see section 2.6). The J_{sc} and FF values of the PNDT-based devices are much higher than those of the PBDT-based devices, which is attributed to differences between the light absorption strengths, charge carrier mobilities, and morphological structures of the active layers.[46]

To determine the origin of the improved J_{sc} of the polymer:$PC_{71}BM$-based device, the external quantum efficiencies (EQEs) of the devices were measured under mono-

DOI: 10.1021/acsami.5b04884
ACS Appl. Mater. Interfaces 2015, 7, 21159−21169

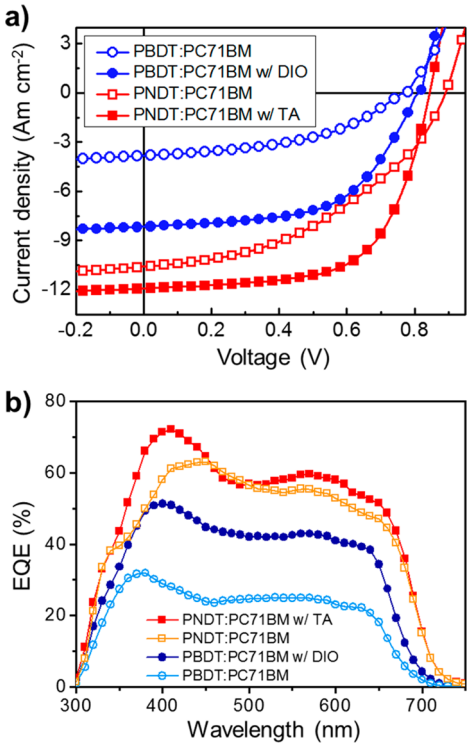

Figure 5. (a) $J-V$ characteristics of polymer:$PC_{71}BM$ solar cells prepared by DCB under illumination of AM 1.5G, 100 mW cm^{-2} and (b) external quantum efficiency curves of the corresponding polymer solar cells.

chromatic light (Figure 5b). The substantially broadened incident photon to current efficiency (IPCE) responses in the visible region of the pristine polymers with respect to their absorption spectra can be attributed to the intrinsic absorptions of the polymers and $PC_{71}BM$. The wavelength ranges of the EQE spectra are in accord with the UV–vis absorption ranges of the polymer:$PC_{71}BM$ blend films (Figure S7, SI). The maximum EQEs of the optimized PNDT-based PSCs (treated with TA) were greater than 70% at 410 nm (overall ~60%), while those of the PBDT-based PSCs (processed with DIO) were ~50% at 400 nm (overall ~40%). The integrated J_{SC} values from the IPCE spectra are 8.1 and 11.9 mA cm^{-2} for PBDT and PNDT, respectively, which are in agreement with the results from the $J-V$ measurements and confirm the reliability of the photovoltaic measurements. The increases in the EQEs upon DIO addition or TA treatment for both polymers are closely related to the strong interchain ordering of the polymer:$PC_{71}BM$ blend films, as was confirmed by the recovery of the strong shoulder peak (originating from interchain $\pi-\pi^*$ transitions) of both blend films in their UV–vis spectra (Figure S7, SI).[14] There is a large variation in the V_{OC} of the PNDT:$PC_{71}BM$-based PSCs (Table 3). This can be attributed to different BHJ morphologies (Figure S8, SI) and thereby different recombination rates of the PNDT:$PC_{71}BM$ blend films, although the V_{OC} can be determined dominantly by the material energetics, ionization potential of donor-electron affinity of acceptor (IP_D-EA_A).[47,48]

2.7. Crystalline Characteristics of Active Layers. To gain a better understanding of the morphological changes upon DIO or TA treatment in the PSC performances, we investigated their film morphologies in detail, in particular, the molecular arrangement/packing and crystalline microstructure, of the polymer:$PC_{71}BM$ blend films by using GIWAXS measurements.[49] The 2D GIWAXS images of the active layers are shown in Figure 6a–d, their line profiles for the out-of-plane (q_z) and in-plane (q_{xy}) directions are shown in Figure 6e,f, and packing parameters were extracted from the GIWAXS profiles and are listed in Table 4. Pronounced (h00) diffraction peaks in the out-of-plane direction are evident for the PBDT:$PC_{71}BM$ blend film, which correspond to a lamellar spacing of 18.2 Å. Upon the addition of DIO, the diffraction patterns become clearer in the out-of-plane direction without noticeable changes in the lamellar spacing, which indicates that the lamellar packing of PBDT is preferentially stacked out of the film plane, i.e., in the "edge-on" molecular orientation.[50] In contrast, the (010) reflections (d^{010} = 3.65 Å) in the out-of-plane direction are clearly detectable for the PNDT:$PC_{71}BM$ blend film treated with TA (Figure 6d), which indicates there is a strong cofacial interchain packing between the neighboring chains as in the "face-on" molecular orientation. Upon TA treatment, the in-plane lamellar diffraction peak is also intensified. The presence of NDT units could induce the coexistence of the face-on lamellar orientation with the edge-on lamellar stacks.[41]

Table 4 shows the lamellar (L_C^{100}) and $\pi-\pi$ stacking (L_C^{010}) correlation lengths of both polymers in their blend films. After blending with $PC_{71}BM$, both polymer:$PC_{71}BM$ films showed enhanced L_C values compared to the neat polymer films (Table 2). The change in film morphology upon adding PCBM molecules results in an enhanced intermolecular interaction of polymer and, thus, in an improved L_C values of polymers.[51] The L_C^{100} values of PBDT and PNDT increased after DIO or TA treatment in the blend films compared to pristine blend films. It appears that PBDT and PNDT undergo strong self-

Table 3. Photovoltaic Properties of Polymer Solar Cells

	treatment						
polymer[a]	DIO[b]	TA[c]	thickness (nm)[d]	V_{oc} (V)	J_{sc} (mA cm^{-2})	FF (%)	PCE_{max} (PCE_{av}) (%)[e]
PBDT	–	–	97	0.76	3.83	46.3	1.35 (1.28)
	yes	–	115	0.86	7.35	65.8	4.15 (4.09)
	–	yes	108	0.82	8.14	56.5	3.78 (3.69)
PNDT	–	–	112	0.90	10.6	43.2	4.12 (4.08)
	yes	–	106	0.68	10.25	55.4	3.86 (3.80)
	–	yes	120	0.84	11.92	63.5	6.35 (6.31)

[a]Polymer:$PC_{71}BM$ blend ratio (w/w) was 1:1. DCB was used as a processing solvent for both polymers. [b]1,8-Diiodooctane (2 vol %) as additive was used. [c]Thermal annealing was performed at 150 °C for 10 min. [d]Thickness of active layer was measured by surface profiler (Alpha-step 500). [e]Performance metrics are average numbers from 12 devices of each type under the illumination condition of AM 1.5G, 100 mW cm^{-2}.

DOI: 10.1021/acsami.5b04884
ACS Appl. Mater. Interfaces 2015, 7, 21159–21169

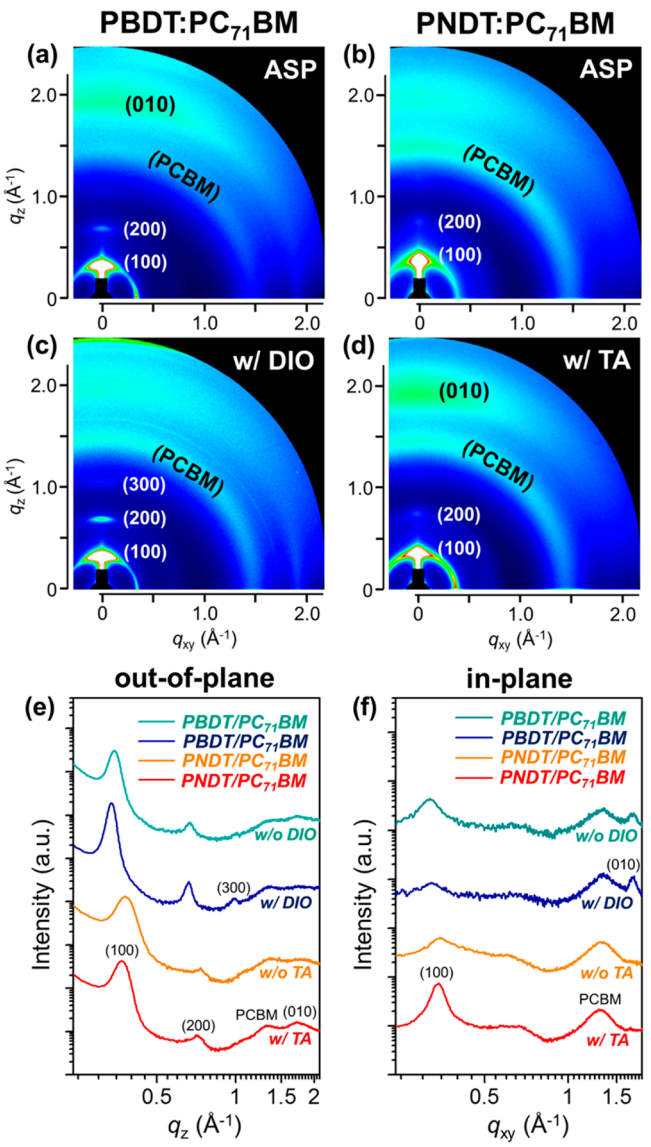

Figure 6. GIWAXS images of polymer:$PC_{71}BM$ blend films prepared by DCB for (a) pristine PBDT and (c) PBDT with DIO and for (b) pristine PNDT and (d) with thermal annealing, respectively. 1D GIWAXS plots of polymer:$PC_{71}BM$ blend films of (e) out-of-plane and (f) in-plane directions.

organization during the film-forming procedure in the blend system upon DIO and TA treatment, respectively.

Interestingly, the L_C^{100} value of PBDT (12.7 nm) was larger than that of PNDT (8.2 nm) in the blend film, which is the reversed trend compared to the neat polymer films. It might be possible that the larger frame of NDT building blocks reduces the ratio of insulating part (alkyl side chains) per conjugated part (NDT-DT2FBT backbone) in the repeat units, providing a more interactive opportunity between PNDT and $PC_{71}BM$ compared to PBDT and $PC_{71}BM$.[52] This could reduce the polymer aggregation ability and lead to lower L_c values of PNDT in the blend films. The hole mobilities of both polymers in their blend films were measured with the space charge limited current (SCLC) method (Table S3, SI).[38] The values of SCLC hole mobilities of both blend systems are in good agreement with the molecular orientations of the polymers; the values increased as the orientation changed from edge-on to face-on.[41] A PBDT:$PC_{71}BM$-based device with DIO shows a higher hole mobility (4.53×10^{-3} cm^2 V^{-1} s^{-1}) than a PNDT:$PC_{71}BM$-based device with TA (2.06×10^{-3} cm^2 V^{-1} s^{-1}), despite PNDT having a face-on orientation. This can be attributed to PBDT having a larger L_C in the blend film than PNDT. Nevertheless, the PCE of the PBDT-based PSC was 4.15%, significantly lower than that of the PNDT-based PSC (6.35%). From the combined results of the PCE and GIWAXS measurements, the difference between the microscopic aspects of the polymer packing structures does not directly correlate with the trend in their photovoltaic performances. Thus, the BHJ morphologies of the active layers blended with $PC_{71}BM$ are also important.

2.8. Morphologies of Active Layers. To gain deeper insight into the effects of the nanoscale morphologies of the photoactive layers on the PCEs, the morphological structures of the polymer:$PC_{71}BM$ blend films were investigated with transmission electron microscopy (TEM) and tapping mode atomic force microscopy (AFM) (Figure 7). As shown in Figure 7a–d (TEM), strongly developed fibrillar structures are evident in both blend films after the DIO or TA treatments. However, relatively larger fibrillar domains were observed in the TEM image (Figure 7b) of the PBDT:$PC_{71}BM$ blend film with DIO compared to that of the PNDT:$PC_{71}BM$ blend film with TA (Figure 7d), which is consistent with the trends in their L_C values obtained from the GIWAXS data (Table 4). With the addition of DIO, $PC_{71}BM$ remains partially dissolved, which affects the diffusive rate of $PC_{71}BM$ in the polymer matrix.[44] In particular, it allows a longer time for PBDT polymer chains to self-organize into highly ordered intermolecular structures. Although the strongly developed fibrillar structures of PBDT in the blend film enhanced the charge transport (Table S3, SI),[29,53,54] they can induce an inefficient exciton dissociation at the PBDT:$PC_{71}BM$ interface due to an unfavorable phase separation with oversized domains.[18] Typically, the exciton diffusion lengths of conjugated polymers are a few nanometers (~10 nm), and hence, the PBDT:$PC_{71}BM$ blend film with DIO, which contains relatively large domains and smaller donor–acceptor interfacial area, produces inefficient exciton diffusion and dissociation, i.e., lower J_{sc} and FF values (Table 3).[55]

Table 4. Crystallographic Information of Photoactive Layers of Optimized Polymer Solar Cells

polymer	treatment	d^{100} (Å)[a]	fwhm^{100} ($Å^{-1}$)[b]	L_C^{100} (nm)[c]	d^{010} (Å)[a]	fwhm^{010} ($Å^{-1}$)[b]	L_C^{010} (nm)[c]
PBDT	none	18.2	0.051	11.07	3.6	0.257	2.20
	DIO	18.6	0.044	12.71	N/A[d]	N/A	N/A
PNDT	none	16.6	0.083	6.74	N/A	N/A	N/A
	TA	17.1	0.068	8.27	3.6	0.283	1.99

[a]Domain spacings of lamellar (d^{100}) and π–π* stacking (d^{010}) in optimized active layers in the out-of-plane (q_z) direction. [b]Full width at half-maximum (fwhm) values. [c]Correlation lengths of lamellar and π–π* stacking crystals using the Scherrer equation. [d]N/A denotes not available.

DOI: 10.1021/acsami.5b04884
ACS Appl. Mater. Interfaces 2015, 7, 21159–21169

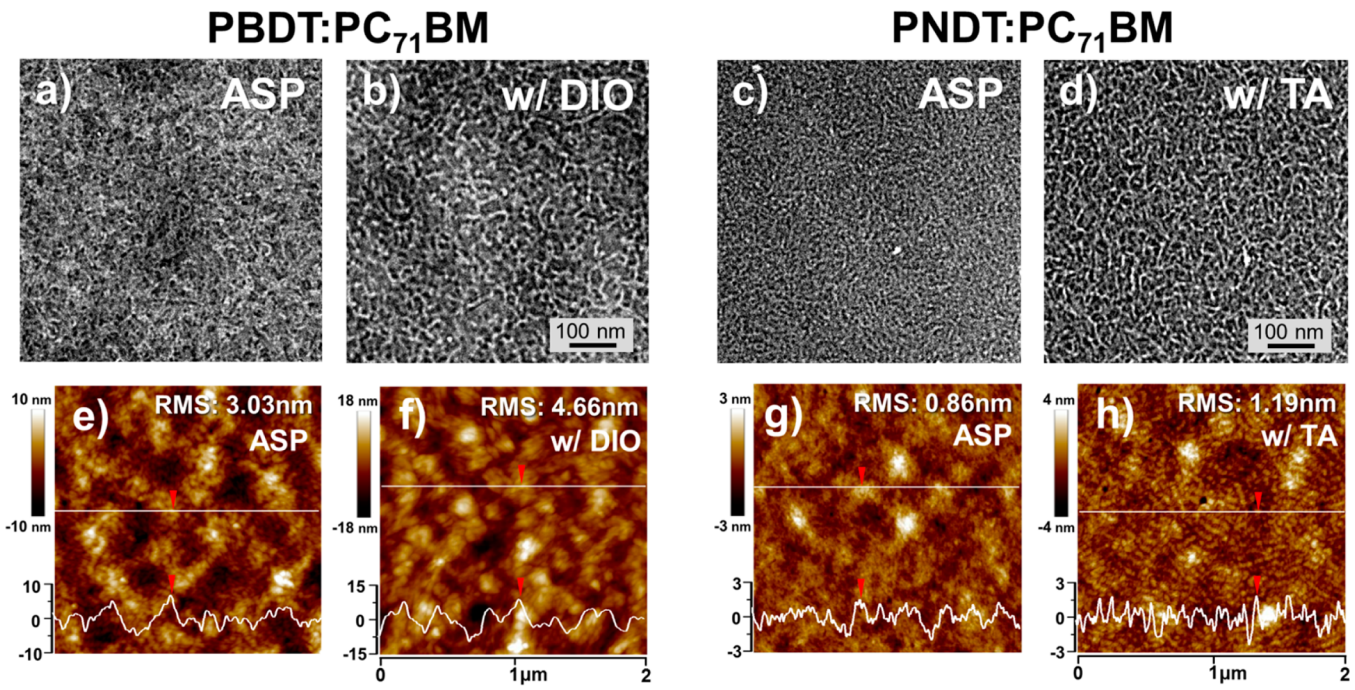

Figure 7. TEM and AFM height images of the polymer:$PC_{71}BM$ blend films based on PBDT (a, b, e, and f) and PNDT (c, d, g, and h). The blend films were prepared using DCB with and without DIO (or TA).

In contrast, a more homogeneous morphology, which contains interpenetrating networks of small-scale polymer-rich (brighter regions) and polymer-deficient (darker regions) domains, is evident in the TEM image (Figure 7d) of the PNDT:$PC_{71}BM$ blend film with TA. The root-mean-square (rms) roughness of the PNDT:$PC_{71}BM$ blend film is much smaller (1.19 nm) than that of PBDT (4.66 nm) according to the AFM topographical images (Figure 7f,h), which indicates the formation of favorable phase separation with nanoscale domains. Two-component mixtures, e.g. polymer and PCBM, often become more miscible as the temperature increase because the entropic gains associated with the component mixing begin to overcome the enthalpic penalties of mixing at higher temperatures.[56] The well-mixed interpenetrating network morphology with small fibrillar domains and large interfacial area of PNDT:$PC_{71}BM$ gives rise to better exciton dissociation, as confirmed by the photoluminescence (PL) quenching efficiency (Figure S8, SI).[57] Thus, we conclude that enhanced light absorption and well-mixed BHJ morphology of PNDT-based device are likely the primary cause of the PCE increase.

3. CONCLUSION

We designed and synthesized two copolymers based on acenedithiophene units (BDT/NDT) as the donor and DT2FBT as the acceptor to explore the effects of extended π-conjugation on D−A copolymers. The NDT polymer has enhanced chain planarity and backbone linearity due to its strong noncovalent interactions and smaller bond angles, which lead to improved light harvesting and charge carrier mobility. The NDT polymer forms a well-distributed interpenetrating nanofibrillar networked BHJ morphology with $PC_{71}BM$ and exhibits less phase separation than the BDT polymer, which results in well-balanced hole and electron mobilities. A conventional optimized device structure PNDT:$PC_{71}BM$ was found to exhibit a maximum solar efficiency of 6.35%, an open-circuit voltage of 0.84 V, a short-circuit current density of 11.92 mA cm^{-2}, and a fill factor of 63.5% after thermal annealing, which demonstrates that the NDT and DT2FBT moieties are a promising electron-donor/acceptor combination for high-performance photovoltaics.

4. EXPERIMENTAL SECTION

4.1. Materials. All reagents were purchased from Aldrich, TCI, and Acros and were used without further purification. All anhydrous organic solvents for the synthesis and device fabrication steps, including tetrahydrofuran (THF), chloroform, toluene, *N*,*N*-dimethylformamide (DMF), chlorobenzene (CB), and 1,2-dichlorobenzene (DCB), were purchased from Aldrich. All reactions were performed with glassware that was oven-dried and then flamed under high vacuum and backfilled with N_2. The monomers 2,6-bis(trimethyltin)-4,8-bis(2-ethylhexyloxy)benzo[1,2-b:3,4-b′]dithiophene, 2,7-bis(trimethyltin)-4,9-bis((2-ethylhexyl)oxy)naphtho[1,2-b:5,6-b′]dithiophene, and 5,6-difluoro-4,7-bis(5-bromo-4-(2-butyloctyl)-2-thienyl)-2,1,3-benzothiadiazole were synthesized according to modified literature procedures.[18,21,28]

4.1.1. Polymer Synthesis. BDT (or NDT) (0.5 mmol) and DT2FBT (0.5 mmol) monomers, $Pd_2(dba)_3$ (8.5 mg), and $P(o\text{-tol})_3$ (12.5 mg) were added to a flame-dried and nitrogen-filled three-neck flask (50 mL). The flask was purged three times with nitrogen, and then degassed chlorobenzene (10 mL) was added. After stirring at 110 °C for 48 h, trimethylthienyltin (0.15 equiv) was added to the reaction flask and the reaction was kept at 110 °C for an additional 3 h. 2-Bromothiophene (0.5 equiv) was then added to the reaction flask, and the temperature was kept at 110 °C for an additional 5 h to complete the end-capping reaction. The mixture was cooled to room temperatures and added dropwise to methanol (300 mL) to obtain a precipitate. After stirring for several hours, the resultant polymer was collected by filtration, dried, and extracted successively with methanol, acetone, and hexane by using a Soxhlet extraction apparatus to remove oligomers and catalyst residue. The remaining solid was extracted with chloroform (150 mL). The chloroform-solution-dissolved polymer was added to an aqueous solution of sodium diethyldithiocarbamate (~1 g/100 mL), and the mixture was heated to 60 °C with vigorous stirring for 6 h to remove residual palladium impurities. After cooling

DOI: 10.1021/acsami.5b04884
ACS Appl. Mater. Interfaces 2015, 7, 21159−21169

to room temperature, the layers were separated, and the organic fraction was washed several times with water (5 × 200 mL).[30] The polymeric solution was further purified by column chromatography with silica gel and Celite using chloroform as eluent. The chloroform fraction was concentrated and precipitated in methanol. The precipitate was filtered and dried in vacuum at 40 °C overnight.

4.1.2. PBDT. Dark brown solid with a metallic luster (345 mg, 81%). GPC: M_n = 27.4 kg mol^{-1}, M_w = 64.6 kg mol^{-1}, PDI = 2.36. ^{1}H NMR (DCB-d_4, 500 MHz, 383 K) δ (ppm): 8.55 (s, 2H), 8.07 (s, 2H), 4.60 (m, 4H), 3.31 (m, 4H), 2.23 (m, 4H), 2.05−1.5 (bm, 48H), 1.21 (m, 12H), 1.11 (m, 12H).

4.1.3. PNDT. Dark brown solid with a metallic luster (380 mg, 75%). GPC: M_n = 33.8 kg mol^{-1}, M_w = 114.9 kg mol^{-1}, PDI = 3.40. ^{1}H NMR (DCB-d_4, 500 MHz) δ (ppm): 8.63−8.09 (br, 2H), 7.87−7.26 (br, 2H), 7.08−6.89 (br, 2H), 4.43−3.91 (br, 8H), 2.38−2.15 (br, 4H), 1.90−1.22 (m, 48H), 0.97−0.33 (m, 24H).

4.2. Characterization. All monomers were characterized by ^{1}H NMR (400 MHz) and ^{13}C NMR (100 MHz) on a Bruker AVANCE 400 spectrometer in chloroform-*d* solutions at room temperature. Number-average ($\overline{M_n}$) and weight-average ($\overline{M_w}$) molecular weights were determined with gel permeation chromatography (GPC, Shimadzu) in chlorobezene at 80 °C, using two PL mixed B columns in series and calibrated against narrow polydispersity polystyrene standards.

4.3. Electrochemistry. CV was conducted on a PowerLab/AD instrument model system with glassy carbon disk, Pt wire, and Ag/Ag$^+$ electrode as the working electrode, counter electrode, and reference electrode, respectively, in a 0.1 M tetrabutylammonium hexafluorophosphate (n-Bu$_4$NPF$_6$)−anhydrous acetonitrile solution at a potential scan rate of 50 mV s^{-1}. Polymer film was drop-cast onto the glassy carbon working electrode from a 2.0 mg mL^{-1} hot DCB solution and dried under house nitrogen stream prior to measurements. The electrochemical onsets were determined at the position where the current starts to differ from the baseline. The potential of Ag/AgCl reference electrode was internally calibrated by using the ferrocene/ferrocenium redox couple (Fc/Fc$^+$). The energy levels were estimated using the equations HOMO = −(4.80 + $E_{onset,ox}$) and LUMO = −(4.80 + $E_{onset,red}$).[28]

4.4. Computational Studies. DFT calculations were performed to facilitate an in-depth understanding of the electronic structure of the polymer by the Gaussian 09 software package. The hybrid three-parameter B3LYP functional combined with 6-31G(d) basis set was used to obtain the optimized structures at the singlet ground state. For simplicity of calculation, the 2-ethylhexyl- and 2-butyloctyl alkyl chains were trimmed with methyl chains. The highest occupied molecular orbital (HOMO) as well as lowest unoccupied molecular orbital (LUMO) energy levels were analyzed using minimized singlet geometries to approximate the ground state.

4.5. Grazing-Incidence Wide-Angle X-ray Scattering (GIWAXS) Analysis. GIWAXS measurements were performed using Beamline 9A at the Pohang Accelerator Laboratory (PAL). The photon energy is 10.6408 keV (λ = 1.1651 Å). The GIWAXS images shown are normalized with respect to exposure time.

4.6. SCLC Measurement. The electron-only devices with (ITO/Al/polymers:PC$_{71}$BM/Al) architecture and the hole-only devices with (ITO/PEDOT:PSS/polymers:PC$_{71}$BM/MoOx/Pd) architecture were fabricated. The electrical characteristics were measured with a source/measure unit (Keithley 4200) in a N$_2$-filled glovebox. The J−V curves were fitted by using the Mott−Gurney square law[58] $J = (9/8)\varepsilon\mu(V^2/L^3)$, where ε is the static dielectric constant of the medium and μ is the carrier mobility.

4.7. Fabrication and Characterization of Organic Field-Effect Transistors (OFETs). A highly n-doped Si (<0.004 Ω cm) substrate was used as a gate electrode. A 300 nm-thick thermally grown oxide layer was employed as a gate dielectric (C_i = 10 nF cm^{-2}). The gate dielectric surface was treated with octadecyltrichlorosilane. Polymers were dissolved in chloroform (10 mg mL^{-1}) and spin-coated onto the substrates at 1500 rpm for 60 s. The devices were completed by evaporating gold through a shadow mask to define source and drain electrodes (80 nm). The channel length (L) and width (W) were 150 μm and 1500 μm, respectively. The electrical characteristic of OFETs was measured in a vacuum using a Keithley 4200 semiconductor parametric analyzer. The field-effect mobility was calculated in the saturation regime (V_D = −60 V) using the following equation: $I_D = {}^1/_2(W/L)\mu C_i(V_G - V_T)$,[39] where I_D is the drain current, μ is the field-effect mobility, and V_G and V_T are the gate voltage and threshold voltage, respectively.

4.8. Fabrication and Characterization of Organic Photovoltaic Devices (OPVs). Indium−tin oxide (ITO)-coated glass substrates were cleaned sequentially with detergent, distilled water, acetone, and isopropyl alcohol. After UV−ozone treatment, poly(3,4-ethylenedioxythiophene)−poly(styrenesulfonate) (PEDOT:PSS, Baytron P VP AI4083, Clevios) was spin-coated on the substrate, which was then baked at 120 °C for 30 min in a convection oven. Polymers and PC$_{71}$BM were dissolved in DCB with various weight ratios and the blend solutions were kept at an elevated temperature (60 °C) for more than 12 h. The polymer:PC$_{71}$BM solutions were spin-coated onto MoO$_3$-deposited substrates, and then the films were left in a N$_2$ atmosphere to dry completely. To deposit the electrodes, the samples were transferred into a vacuum chamber (pressure <1 × 10^{-6} Torr), and then LiF (0.6 nm)/Al(100 nm) were deposited sequentially in a conventional structure on top of the thin films by thermal evaporation. The electrical characteristics were measured with a source/measure unit (Keithley 4200) in the dark and under 100 mW cm^{-2} AM1.5 solar illumination in a N$_2$-filled glovebox. Light was generated with an Oriel 1 kW solar simulator referenced using a PVM 132 reference cell calibrated at the US National Renewable Energy Laboratory. A photomodulation spectroscopic setup (model Merlin, Oriel) was used to measure the incident photon-to-current conversion efficiency as a function of light wavelength. The device area was 0.0555 cm^2.

■ ASSOCIATED CONTENT

Supporting Information

The Supporting Information is available free of charge on the ACS Publications website at DOI: 10.1021/acsami.5b04884.

Schemes S1 and S2, Figures S1−S9, and Tables S1−S3; synthetic procedures of monomers; H^1 and C^{13} NMR spectra of monomers; DFT analysis of model compounds; the current−voltage characteristics of the OFETs; UV−vis absorption spectra, photoluminescence spectra, and AFM and TEM images of the polymer:PC$_{71}$BM blend films; the photovoltaic properties and SCLC mobilities of PSCs with various fabrication conditions (PDF)

■ AUTHOR INFORMATION

Corresponding Author

*E-mail: kwcho@postech.ac.kr.

Author Contributions

J.L. and H.K. contributed equally to this work.

Notes

The authors declare no competing financial interest.

■ ACKNOWLEDGMENTS

This work was supported by a grant (Code No. 2011-0031628) from the Center for Advanced Soft Electronics under the Global Frontier Research Program of the Ministry of Science, ICT & Future Planning, Korea. The authors thank the Pohang Accelerator Laboratory for providing the synchrotron radiation sources at 9A beamline used in this study.

■ REFERENCES

(1) Wu, J.; Cheng, S. W.; Cheng, Y. J.; Hsu, C. S. Donor−Acceptor Conjugated Polymers Based on Multifused Ladder-Type Arenes for Organic Solar Cells. *Chem. Soc. Rev.* **2015**, *44*, 1113−1154.

(2) Liang, Y.; Yu, L. A New Class of Semiconducting Polymers for Bulk Heterojunction Solar Cells with Exceptionally High Performance. *Acc. Chem. Res.* **2010**, *43*, 1227−1236.
(3) Darling, S. B.; You, F. The Case for Organic Photovoltaics. *RSC Adv.* **2013**, *3*, 17633−17648.
(4) Kippelen, B.; Bredas, J.-L. Organic Photovoltaics. *Energy Environ. Sci.* **2009**, *2*, 251−261.
(5) Coakley, K. M.; McGehee, M. D. Conjugated Polymer Photovoltaic Cells. *Chem. Mater.* **2004**, *16*, 4533−4542.
(6) He, Z.; Zhong, C.; Su, S.; Xu, M.; Wu, H.; Cao, Y. Enhanced Power-Conversion Efficiency in Polymer Solar Cells using an Inverted Device Structure. *Nat. Photonics* **2012**, *6*, 591−595.
(7) Kim, M.; Park, J. H.; Kim, J.-H.; Sung, J. H.; Jo, S. B.; Jo, M.-H.; Cho, K. Lateral Organic Solar Cells with Self-Assembled Semiconductor Nanowires. *Adv. Energy Mater.* **2015**, *5*, DOI: 10.1002/aenm.201570023.
(8) Love, J. A.; Collins, S. D.; Nagao, I.; Mukherjee, S.; Ade, H.; Bazan, G. C.; Nguyen, T.-Q. Interplay of Solvent Additive Concentration and Active Layer Thickness on the Performance of Small Molecule Solar Cells. *Adv. Mater.* **2014**, *26*, 7308−7316.
(9) Adams, J.; Spyropoulos, G. D.; Salvador, M.; Li, N.; Strohm, S.; Lucera, L.; Langner, S.; Machui, Fl.; Zhang, H.; Ameri, T.; Voigt, M. M.; Krebs, F. C.; Brabec, C. J. Air-Processed Organic Tandem Solar Cells on Glass: Toward Competitive Operating Lifetimes. *Energy Environ. Sci.* **2015**, *8*, 169−176.
(10) Peet, J.; Kim, J. Y.; Coates, N. E.; Ma, W. L.; Moses, D.; Heeger, A. J.; Bazan, G. C. Efficiency Enhancement in Low-Bandgap Polymer Solar Cells by Processing with Alkane Dithiols. *Nat. Mater.* **2007**, *6*, 497−500.
(11) Kim, J.-H.; Kim, M.; Jinnai, H.; Shin, T. J.; Kim, H.; Park, J. H.; Jo, S. B.; Cho, K. Organic Solar Cells Based on Three-Dimensionally Percolated Polythiophene Nanowires with Enhanced Charge Transport. *ACS Appl. Mater. Interfaces* **2014**, *6*, 5640−5650.
(12) Liu, Y.; Zhao, J.; Li, Z.; Mu, C.; Ma, W.; Hu, H.; Jiang, K.; Lin, H.; Ade, H.; Yan, H. Aggregation and Morphology Control Enables Multiple Cases of High-Efficiency Polymer Solar Cells. *Nat. Commun.* **2014**, *5*, 5293.
(13) Dou, L.; Chen, C.; Yoshimura, K.; Ohya, K.; Chang, W.; Gao, J.; Liu, Y.; Richard, E.; Yang, Y. Synthesis of 5H-Dithieno[3,2-b:2′,3′-d]pyran as an Electron-Rich Building Block for Donor−Acceptor Type Low-Bandgap Polymers. *Macromolecules* **2013**, *46*, 3384−3390.
(14) Nguyen, T. L.; Choi, H.; Ko, S.-J.; Uddin, M. A.; Walker, B.; Yum, S.; Jeong, J.-E.; Yun, M. H.; Shin, T. J.; Hwang, S.; Kim, J. Y.; Woo, H. Y. Semi-Crystalline Photovoltaic Polymers with Efficiency Exceeding 9% in a 300 nm Thick Conventional Single-Cell Device. *Energy Environ. Sci.* **2014**, *7*, 3040−3051.
(15) Ye, L.; Zhang, S.; Huo, L.; Zhang, M.; Hou, J. Molecular Design toward Highly Efficient Photovoltaic Polymers Based on Two-Dimensional Conjugated Benzodithiophene. *Acc. Chem. Res.* **2014**, *47*, 1595−1603.
(16) Osaka, I.; Shinamura, S.; Abe, T.; Takimiya, T. Naphthodithiophenes as Building Units for Small Molecules to Polymers; A Case Study for In-Depth Understanding of Structure−Property Relationships in Organic Semiconductors. *J. Mater. Chem. C* **2013**, *1*, 1297−1304.
(17) Payne, M. M.; Parkin, S. R.; Anthony, J. E.; Kuo, C.-C.; Jackson, T. N. Organic Field-Effect Transistors from Solution-Deposited Functionalized Acenes with Mobilities as High as 1 $cm^2/V{\cdot}s$. *J. Am. Chem. Soc.* **2005**, *127*, 4986−4987.
(18) Lee, J.; Kim, M.; Kang, B.; Jo, S. B.; Kim, H. G.; Shin, J.; Cho, K. Side-Chain Engineering for Fine-Tuning of Energy Levels and Nanoscale Morphology in Polymer Solar Cells. *Adv. Energy Mater.* **2014**, *4*, DOI: 10.1002/aenm.201470054.
(19) Cui, C.; Wong, W.-Y.; Li, Y. Improvement of Open-Circuit Voltage and Photovoltaic Properties of 2D-Conjugated Polymers by Alkylthio Substitution. *Energy Environ. Sci.* **2014**, *7*, 2276−2284.
(20) Guo, X.; Tsao, H. N.; Gao, P.; Xia, D.; An, C.; Nazeeruddin, M. K.; Baumgarten, M.; Grätzel, M.; Müllen, K. Dithieno[2,3-d;2′,3′-d′]benzo[1,2-b;4,5-b′]-dithiophene based Organic Sensitizers for Dye-Sensitized Solar Cells. *RSC Adv.* **2014**, *4*, 54130−54133.
(21) Loser, S.; Miyauchi, H.; Hennek, J. W.; Smith, J.; Huang, C.; Facchetti, A.; Marks, T. J. A "Zig-Zag" Naphthodithiophene Core for Increased Efficiency in Solution-Processed Small Molecule Solar Cells. *Chem. Commun.* **2012**, *48*, 8511−8513.
(22) Peng, Q.; Huang, Q.; Hou, X.; Chang, P.; Xu, J.; Deng, S. Enhanced Solar Cell Performance by Replacing Benzodithiophene with Naphthodithiophene in Diketopyrrolopyrrole-Based Copolymers. *Chem. Commun.* **2012**, *48*, 11452−11454.
(23) Cheng, S.-W.; Chiou, D.-Y.; Lai, Y.-Y.; Yu, R.-H.; Lee, C.-H.; Cheng, Y.-J. Synthesis and Molecular Properties of Four Isomeric Dialkylated Angular-Shaped Naphthodithiophenes. *Org. Lett.* **2013**, *15*, 5338−5341.
(24) Osaka, I.; Abe, T.; Shinamura, S.; Takimiya, L. Impact of Isomeric Structures on Transistor Performances in Naphthodithiophene Semiconducting Polymers. *J. Am. Chem. Soc.* **2011**, *133*, 6852−6860.
(25) Osaka, I.; Kakara, T.; Takemura, N.; Koganezawa, T.; Takimiya, K. Naphthodithiophene−Naphthobisthiadiazole Copolymers for Solar Cells: Alkylation Drives the Polymer Backbone Flat and Promotes Efficiency. *J. Am. Chem. Soc.* **2013**, *135*, 8834−8837.
(26) Zhu, X.; Fang, J.; Lu, K.; Zhang, J.; Zhu, L.; Zhao, Y.; Shuai, Z.; Wei, Z. Naphtho[1,2-b:5,6-b′]dithiophene Based Two-Dimensional Conjugated Polymers for Highly Efficient Thick-Film Inverted Polymer Solar Cells. *Chem. Mater.* **2014**, *26*, 6947−6954.
(27) Peng, Q.; Liu, X.; Su, D.; Fu, G.; Xu, J.; Dai, L. Novel Benzo[1,2-b:4,5-b]dithiophene−Benzothiadiazole Derivatives with Variable Side Chains for High-Performance Solar Cells. *Adv. Mater.* **2011**, *23*, 4554−4558.
(28) Zhou, H.; Yang, L.; Stuart, A. C.; Price, S. C.; Liu, S.; You, W. Development of Fluorinated Benzothiadiazole as a Structural Unit for a Polymer Solar Cell of 7% Efficiency. *Angew. Chem., Int. Ed.* **2011**, *50*, 2995−2998.
(29) Lee, J.; Jo, S. B.; Kim, M.; Kim, H. G.; Shin, J.; Kim, H.; Cho, K. Donor−Acceptor Alternating Copolymer Nanowires for Highly Efficient Organic Solar Cells. *Adv. Mater.* **2014**, *26*, 6706−6714.
(30) Bronstein, H.; Frost, J. M.; Hadipour, A.; Kim, Y.; Nielsen, C. B.; Ashraf, R. S.; Rand, B. P.; Watkins, S.; McCulloch, I. Effect of Fluorination on the Properties of a Donor−Acceptor Copolymer for Use in Photovoltaic Cells and Transistors. *Chem. Mater.* **2013**, *25*, 277−285.
(31) Kim, J. S.; Fei, Z.; Wood, S.; James, D. T.; Sim, M.; Cho, K.; Heeney, M. J.; Kim, J.-S. Germanium- and Silicon-Substituted Donor−Acceptor Type Copolymers: Effect of the Bridging Heteroatom on Molecular Packing and Photovoltaic Device Performance. *Adv. Energy Mater.* **2014**, *4*, 1400527.
(32) Ren, Y.; Hailey, A. K.; Hiszpanski, A. M.; Loo, Y.-L. Isoindigo-Containing Molecular Semiconductors: Effect of Backbone Extension on Molecular Organization and Organic Solar Cell Performance. *Chem. Mater.* **2014**, *26*, 6570−6577.
(33) Hou, J.; Chen, H. Y.; Zhang, S.; Chen, R. I.; Yang, Y.; Wu, Y.; Li, G. Synthesis of a Low Band Gap Polymer and Its Application in Highly Efficient Polymer Solar Cells. *J. Am. Chem. Soc.* **2009**, *131*, 15586−15587.
(34) Lee, C. T.; Yang, W. T.; Parr, R. G. Development of the Colle-Salvetti Correlation-Energy Formula into a Functional of the Electron Density. *Phys. Rev. B: Condens. Matter Mater. Phys.* **1988**, *37*, 785−789.
(35) Xu, Y.-X.; Chueh, C.-C.; Yip, H.-L.; Ding, F.-Z.; Li, Y.-X.; Li, C.-Z.; Li, X.; Chen, W.-C.; Jen, A. K.-Y. Improved Charge Transport and Absorption Coefficient in Indacenodithieno[3,2-b]thiophene-based Ladder-Type Polymer Leading to Highly Efficient Polymer Solar Cells. *Adv. Mater.* **2012**, *24*, 6356−6361.
(36) Darling, S. B.; Sternberg, M. Importance of Side Chains and Backbone Length in Defect Modeling of Poly(3-alkylthiophenes). *J. Phys. Chem. B* **2009**, *113*, 6215−6218.
(37) Jackson, N. E.; Savoie, B. M.; Kohlstedt, K. L.; Olvera de la Cruz, M.; Schatz, G. C.; Chen, L. X.; Ratner, M. A. Controlling Conformations of Conjugated Polymers and Small Molecules: The

DOI: 10.1021/acsami.5b04884
ACS Appl. Mater. Interfaces 2015, 7, 21159−21169

Role of Nonbonding Interactions. *J. Am. Chem. Soc.* **2013**, *135*, 10475−10483.
(38) Goodman, A. M.; Rose, A. Double Extraction of Uniformly Generated Electron-Hole Pairs from Insulators with Noninjecting Contacts. *J. Appl. Phys.* **1971**, *42*, 2823−2830.
(39) Lim, J. A.; Kim, J.-H.; Qiu, L.; Lee, W. H.; Lee, H. S.; Kwak, D.; Cho, K. Inkjet-Printed Single-Droplet Organic Transistors Based on Semiconductor Nanowires Embedded in Insulating Polymers. *Adv. Funct. Mater.* **2010**, *20*, 3292−3297.
(40) Shaw, J.; Zhong, H.; Yau, C. P.; Casey, A.; Buchaca-Domingo, E.; Stingelin, N.; Sparrowe, D.; Mitchell, W.; Heeney, M. Alternating Copolymers Incorporating Dithienogemolodithiophene for Field-Effect Transistor Applications. *Macromolecules* **2014**, *47*, 8602−8610.
(41) Wu, Y.; Li, Z.; Ma, W.; Huang, Y.; Huo, L.; Guo, X.; Zhang, M.; Ade, H.; Hou, J. PDT-S-T: A New Polymer with Optimized Molecular Conformation for Controlled Aggregation and $\pi-\pi$ Stacking and Its Application in Efficient Photovoltaic Devices. *Adv. Mater.* **2013**, *25*, 3449−3455.
(42) Rivnay, J.; Mannsfeld, S. C. B.; Miller, C. E.; Salleo, A.; Toney, M. F. Quantitative Determination of Organic Semiconductor Microstructure from the Molecular to Device Scale. *Chem. Rev.* **2012**, *112*, 5488−5519.
(43) Kim, K. H.; Park, S.; Yu, H.; Kang, H.; Song, I.; Oh, J. H.; Kim, B. J. Determining Optimal Crystallinity of Diketopyrrolopyrrole-Based Terpolymers for Highly Efficient Polymer Solar Cells and Transistors. *Chem. Mater.* **2014**, *26*, 6963−6970.
(44) Liu, F.; Zhao, W.; Tumbleston, J. R.; Wang, C.; Gu, Y.; Wang, D.; Briseno, A. L.; Ade, H.; Russell, T. P. Understanding the Morphology of PTB7:PCBM Blends in Organic Photovoltaics. *Adv. Energy Mater.* **2014**, *4*, 1301377.
(45) Liao, H.-C.; Ho, C.-C.; Chang, C.-Y.; Jao, M.-H.; Darling, S. B.; Su, W.-F. Additives for Morphology Control in High-Efficiency Organic Solar Cells. *Mater. Today* **2013**, *16*, 326−336.
(46) Liang, Y.; Wu, Y.; Feng, D.; Tsai, S.-T.; Son, H.-J.; Li, G.; Yu, L. Development of New Semiconducting Polymers for High Performance Solar Cells. *J. Am. Chem. Soc.* **2009**, *131*, 56−57.
(47) Credgington, D.; Durrant, J. R. Insights from Transient Optoelectronic Analyses on the Open-Circuit Voltage of Organic Solar Cells. *J. Phys. Chem. Lett.* **2012**, *3*, 1465−1478.
(48) Perez, M. D.; Borek, C.; Forrest, S. R.; Thompson, M. E. Molecular and Morphological Influences on the Open Circuit Voltages of Organic Photovoltaic Devices. *J. Am. Chem. Soc.* **2009**, *131*, 9281−9286.
(49) Chen, W.; Nikiforov, M. P.; Darling, S. B. Morphology Characterization in Organic and Hybrid Solar Cells. *Energy Environ. Sci.* **2012**, *5*, 8045−8074.
(50) Kim, D. H.; Park, Y. D.; Jang, Y.; Yang, H.; Kim, Y. H.; Han, J. I.; Moon, D. G.; Park, S.; Chang, T.; Joo, M.; Ryu, C. Y.; Cho, K. Enhancement of Field-Effect Mobility Due to Surface-Mediated Molecular Ordering in Regioregular Polythiophene Thin Film Transistors. *Adv. Funct. Mater.* **2005**, *15*, 77−82.
(51) Mihailetchi, V. D.; Koster, L. J. A.; Blom, P. W. M.; Melzer, C.; de Boer, B.; van Duren, J. K. J.; Janssen, R. A. J. Compositional Dependence of the Performance of Poly(p-phenylene vinylene):Methanofullerene Bulk-Heterojunction Solar Cells. *Adv. Funct. Mater.* **2005**, *15*, 795−801.
(52) Kim, J.-H.; Park, J. B.; Xu, F.; Kim, D.; Kwak, J.; Grimsdale, A. C.; Hwang, D.-H. Effect of π-Conjugated Bridges of TPD-Based Medium Bandgap Conjugated Copolymers for Efficient Tandem Organic Photovoltaic. Cells. *Energy Environ. Sci.* **2014**, *7*, 4118−4131.
(53) Subramaniyan, S.; Xin, H.; Kim, F. S.; Murari, N. M.; Courtright, B. A. E.; Jenekhe, S. A. Thiazolothiazole Donor−Acceptor Conjugated Polymer Semiconductors for Photovoltaic Applications. *Macromolecules* **2014**, *47*, 4199−4209.
(54) Kim, J. S.; Lee, J. H.; Park, J. H.; Shim, C.; Sim, M.; Cho, K. High-Efficiency Organic Solar Cells Based on Preformed Poly(3-hexylthiophene) Nanowires. *Adv. Funct. Mater.* **2011**, *21*, 480−486.
(55) Li, W.; Hendriks, K. H.; Furlan, A.; Roelofs, W. S. C.; Meskers, S. C. J.; Wienk, M. M.; Janssen, R. A. J. Effect of the Fibrillar Microstructure on the Efficiency of High Molecular Weight Diketopyrrolopyrrole-Based Polymer Solar Cells. *Adv. Mater.* **2014**, *26*, 1565−1570.
(56) Collins, B. A.; Gann, E.; Guignard, L.; He, X.; McNeill, C. R.; Ade, H. Molecular Miscibility of Polymer−Fullerene Blends. *J. Phys. Chem. Lett.* **2010**, *1*, 3160−3166.
(57) Liao, H.; Tsao, C.; Shao, Y.; Chang, S.; Huang, Y.; Chuang, C.; Lin, T.; Chen, C.; Su, C.; Jeng, U.; Chen, Y.; Su, W. Bi-Hierarchical Nanostructures of Donor−Acceptor Copolymer and Fullerene for High Efficient Bulk Heterojunction Solar Cells. *Energy Environ. Sci.* **2013**, *6*, 1938−1948.
(58) Mott, N. F.; Gurney, R. W. *Electronic Processes in Ionic Crystals*, 1st ed; Oxford University Press: London, 1940.

DOI: 10.1021/acsami.5b04884
ACS Appl. Mater. Interfaces 2015, 7, 21159−21169